ELSEVIER

Journal of Nuclear Materials 290–293 (2001) 1185–1189

journal of nuclear materials

www.elsevier.nl/locate/jnucmat

Overview of impurity control and wall conditioning in NSTX

H.W. Kugel [a,*], R. Maingi [b], W. Wampler [g], R.E. Barry [b], M. Bell [a], W. Blanchard [a], D. Gates [a], D. Johnson [a], R. Kaita [a], S. Kaye [a], R. Maqueda [c], J. Menard [a], M.M. Menon [b], D. Mueller [a], M. Ono [a], S. Paul [a], Y-K.M. Peng [b], R. Raman [d], A. Roquemore [a], C.H. Skinner [a], S. Sabbagh [e], B. Stratton [a], D. Stutman [f], J.R. Wilson [a], S. Zweben [a], NSTX National Research Team

[a] *Princeton Plasma Physics Laboratory, Princeton, NJ 08543, USA*
[b] *Oak Ridge National Laboratory, Oak Ridge, TN 37831, USA*
[c] *Los Alamos National Laboratory, Los Alamos, NM 87545, USA*
[d] *University of Washington, Seattle, WA 98195, USA*
[e] *Columbia University, New York, NY 10027, USA*
[f] *Johns Hopkins University, Baltimore, MD 21218, USA*
[g] *Sandia National Laboratories, Albuquerque, NM 87123, USA*

Abstract

The national spherical torus experiment (NSTX) started plasma operations in February 1999. In the first extended period of experiments, NSTX achieved high current, inner wall limited, double null, and single null plasma discharges, initial Coaxial Helicity Injection, and high harmonic fast wave results. As expected, discharge reproducibility and performance were strongly affected by wall conditions. In this paper, we describe the internal geometry, and initial plasma discharge, impurity control, wall conditioning, erosion, and deposition results. © 2001 Elsevier Science B.V. All rights reserved.

Keywords: Wall conditioning; Impurity control; Glow discharge cleaning

1. Introduction

In February 1999, the national spherical torus experiment (NSTX) achieved first plasma. In the first extended period of experiments, it promptly achieved high plasma current, in inner wall limited, double null, and single null plasma configurations. 130 kA of initial non-inductive current generation using 20 kA of Coaxial Helicity Injection (CHI) current has been demonstrated, and indications of electron heating with 2 MW of high harmonic fast wave RF heating (HHFW) have been obtained [1].

The device capabilities include $R_0 \leqslant 0.85$ m, $a \leqslant 0.67$ m, $R/a \geqslant 1.26$, $\kappa \leqslant 2.2$, $\delta < 0.5$, $I_p \leqslant 1$ MA, $B_T \leqslant 0.3$ T, and 5 s maximum pulse length. Copper passive stabilizer plates, graphite power handling surfaces, 5 MW of neutral beam heating (October 2000), 6 MW of 30 MHz high harmonic fast wave (HHFW) for heating and current drive at 10–20 ω_{ICRF}. The 0.2 m radius center column is clad with alternating vertical columns of 1.3 cm thick graphite (Union Carbide, Type ATJ) tiles between columns of 2-D Carbon Fiber Composite (CFC) (Allied Signal, Type 865-19-4) tiles. The inner divertor tiles are 5.1 cm thick graphite; the outer divertor and passive stabilizer plate tiles are 2.5 cm thick graphite. A unique feature of NSTX: toroidal ceramic insulators, in the top and bottom divertor gaps, which allows for electrical biasing of the inner and outer vessel for CHI. This configuration enables experiments with ohmic, neutral beam and HHFW heated discharges on wall

* Corresponding author. Tel.: +1-609 243 3146; fax: +1-609 243 3248.
E-mail address: hkugel@pppl.gov (H.W. Kugel).

PII: S0022-3115(00)00496-7

limiter start-up plasmas, lower single-null diverted plasmas, and double null diverted plasmas with and without CHI [2,3].

NSTX is expected to produce plasma boundary regimes and plasma surface interactions similar to tokamaks but with significant differences [2,3]. Fig. 1 shows how the ST magnetic field line geometry differs from that of a conventional large aspect ratio tokamak. In the case of inner wall limited discharges, for example, the field in the Scrape-Off Layer (SOL) varies by a factor of 4 and in diverted discharges by a factor of 2. This results in large reflected and trapped ion flux in the SOL. This reflection of trapped ion flux increases the effective parallel connection length in a collisionless edge plasma. Collisions reduce the effect of this trapping. Since the width of the SOL is determined by the ratio of the parallel to perpendicular transport, the longer parallel connection length may cause a wider SOL in the ST as the edge plasma becomes less collisional. However, during neutral beam heating, under some conditions (e.g. lower I_p), substantial ion loss may occur from large ion orbits in the outer region of bad curvature which could increase the perpendicular transport and tend to shorten the SOL. In addition, on inner wall surfaces, flux expansion ratios of ~10 in the SOL for ST inner wall limited discharges will lower the effective incident power densities. In the outer region, however, the field line pitch of about 45° results in a short outer connection length from the midplane to the inner wall, and even shorter to the divertor plates for diverted discharges. Simulations indicate that at full power (11 MW) and full pulse length (5 s), divertor power densities will be about 7 MW/m^2 yielding tile peak front face temperatures of 1200°C. Although these temperature rises are below the regime where radiation enhanced sublimation would be expected to instigate carbon blooms, this may no longer be the case as surfaces become micro-fractured and eroded due to intense ion bombardment [3–5].

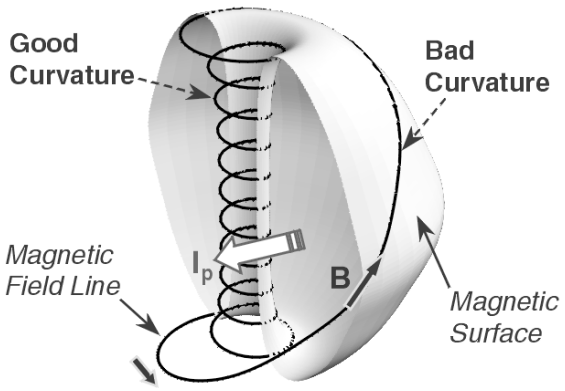

Fig. 1. Schematic of spherical torus (ST) magnetic field line geometry.

2. Wall conditioning for first plasma start-up in February 1999 with few internal components

The initial configuration for first plasma start-up in February 1999 consisted of the stainless steel vacuum vessel (volume, 30 m^3; area, 54 m^2 ; D_2 pumping speed 3368l s^{-1}), the center column partially clad (50%) with graphite, and a small graphite outer bumper limiter. The passive stabilizer plates were not yet installed and there was no graphite on the outer divertors. The initial vessel evacuation started in mid November 1998. At that time the bakeout system was not functional. In order to remove water, CO, CO_2, and hydrocarbons as rapidly as possible so as to meet the start-up schedule, about 39 h of D_2GDC was performed at room temperature. This was followed by 4 h of HeGDC to remove residual D_2. A preliminary GDC system was used for this process. This consisted of a moveable stainless steel anode and a biased preionization filament for initiating GDC at the actual operating pressure and voltage (2 mTorr for D_2 and 4 mTorr for He at 400 V). Starting at the actual operating pressure and voltage was done to reduce violent arcing and sputtering events, and to reduce stress on the torus vacuum pumping system which was kept in the normal high vacuum mode during GDC. Fig. 2 shows a comparison of D_2GDC wall impurity cleaning followed by HeGDC wall conditioning to remove the residual D_2. It is seen that D_2GDC was very effective for removing impurities from the walls. HeGDC was found much less efficient for removing impurities but was

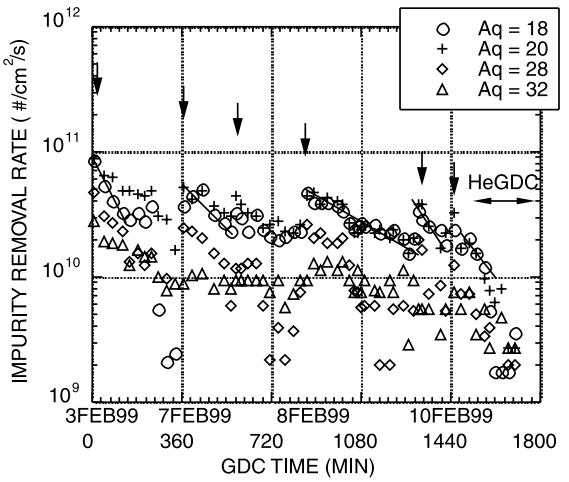

Fig. 2. Comparison of D_2GDC impurity cleaning followed by HeGDC wall conditioning for February 1999 vessel configuration with few internal components. The arrows indicate the start of each D_2GDC application after a period of no GDC. D_2GDC was very effective for removing impurities from the walls. HeGDC was used to remove residual D_2. The solid lines are a guide to show the trend of the GDC.

found very effective for removing residual D_2. The first plasma discharge was limited to about 20 kA. Subsequently, the biased pre-ionization filament was applied to assist plasma breakdown, and over a 1.5 day period, discharges were readily obtained up to 280 kA with about 1/3 of the available OH flux.

3. Wall conditioning after August 1999 for 1 MA plasmas with full internal components

After a 5 month opening to install additional hardware, NSTX was evacuated in early August 1999 with a nearly complete internal configuration which included a divertor region clad 100% with graphite tiles, and copper passive stabilizer plates clad 50% with graphite tiles. Other internal hardware installations included a double fixed anode GDC system with two biased filaments which allowed GDC initiation at the operating pressure and voltage [6]. In view of the extensive construction that had taken place in the vessel during the 5 month vent, and the need to quickly remove residual impurities, about 140 h of D_2GDC was performed at room temperature to remove water, CO, CO_2 and hydrocarbons, and about 20 h of HeGDC to remove residual D_2. This was followed by a 206°C bakeout of the center column performed using resistive heating, during which 10 h of D_2GDC and 12 h of HeGDC were performed. In September 1999, operations resumed, and plasma discharges of over 800 kA were achieved relatively quickly. An additional extended bakeout experiment in November 1999 was performed at increasing higher temperatures during which the center column was heated to 309°C and the passive stabilizer to about 220°C. Fig. 3 shows removal rates of the mass 18, 28 and 44 impurity components.

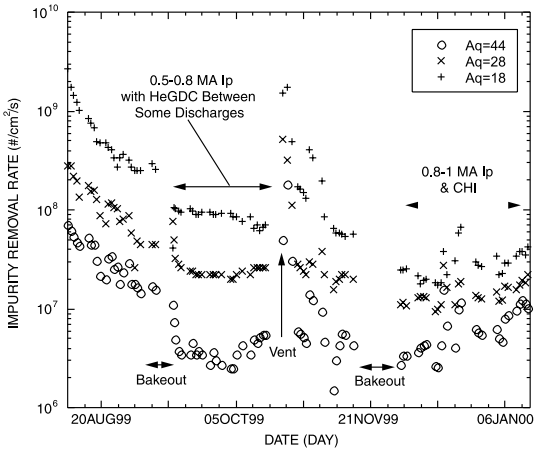

Fig. 3. Removal rates for the mass 18, 28, and 44 impurity components as walls were conditioned using D_2GDC, HeGDC, and bakeout to prepare NSTX for 1 MA Discharges.

During this D_2GDC and HeGDC cleaning procedure, the vessel windows were not covered. The light transmission of an exposed midplane window near a GDC wall anode was measured after GDC, bakeout, and low ohmic power plasma operations ($I_p \sim\leqslant 500$ kA). The transmission in the visible was found to decrease about 5% per 10 h of D_2 or HeGDC at room temperature. Measurements of the thickness and elemental composition of the coating on an exposed window indicated that the depositions prior to CHI and Ohmic discharges with $I_p > 0.5$ MA was $\sim<$ 550 Å thick with the following composition: H (18.3%), C (15.0%), O (24.0%), Cr (5.5%), Fe (23.0%), Cu (12.0%), and Mo (0.20%). No deuterium was observed even though only deuterium plasmas were used (no hydrogen plasmas were ever used). Hence, the hydrogen content is attributed to hydrogenated components residual in the tiles which outgasssed during discharges. Relatively little carbon was observed even though there was an extensive graphite surface. The deposition appeared to be mostly metal oxides. Visible window transmissions measured at other toroidal locations increased systematically as the distance from the GDC wall anodes increased, indicating some enhanced local deposition near the GDC anodes.

4. Wall evolution and surface analysis results

After the final bakeout in November 1999, improved wall conditions and advances in control technique allowed higher current discharges to $I_p > 0.9$ MA for 70 ms ($W_{tot} = 31$ kJ, $\beta_t = 5.6\%$, $\tau_e = 15$ ms, $n_e \sim\leqslant 2.8 \times 10^{13}$ cm^{-3}), and by December 14, 1999, 1 MA discharges were attained with ramp-rates of up to 7 MA/s [7]. In these discharges, electron cyclotron preionization (18 GHz, 30 kW) and biased filament preionization were used routinely to assist discharge initiation.

During ohmic operations, about 40 discharges were required to achieve low reproducible D_α edge light emission. In general, the application of HeGDC between discharges had no systematic impact on plasma recycling and plasma performance in the flat-top region. However, HeGDC was useful if the plasma had start-up problems. In special cases, for example, following initial CHI experiments [8], 30 min of HeGDC was performed, and it then took ~10 single-null discharges to reduce visible light emission from D_α, carbon, and oxygen back to pre-CHI levels. After this, performing 5 min of HeGDC between discharges made a step change (~10%) to achievable plasma current and/or flattop duration; subsequent 5 min HeGDC between discharges exhibited no improvement in plasma performance. In other discharge sequences, the recycling/visible light baseline was

reduced by only up to 10% after 3 HeGDC/plasma discharge sequences (Fig. 4). The $(H_\alpha/H_\alpha + D_\alpha)$ ratio, which is important to minimize in NSTX so as to avoid parasitic HHFW resonance, was about 95% before the October 1999 bakeout but reached less than 10% by the end of the campaign during gas puffed discharges. Initial visible spectroscopic measurements indicated moderate levels of low-Z impurities that tended to increase with discharge number during a given operating day. Bolometer measurements on similar discharges indicated radiative power fractions in the range 0.25–0.30. However, in other discharges, filtered soft-Xray measurements of plasma profiles indicated that metallic impurities due to exposed copper and stainless steel were often high [9].

Erosion and deposition were studied using sample coupons and silicon marker implants. Given the wide range of experiments and tests that were performed during the Startup phase, the erosion and deposition that occurred cannot be related to specific conditions at this time. However, the approximate operating time was the sum of about 1125 discharges, during 41 plasma operation days with nearly 30 discharges per day, typically of ~100 ms duration, and in addition, several days of special CHI experiments of up to 130 ms duration were performed. For this work, four stainless steel and two silicon sample coupons (2.5×2.5 cm^2) were mounted at the midplane at four toroidal locations on the outer vessel wall about 10 cm beyond the SOL of the most outward plasma. In addition, 12 stainless steel coupons were positioned in a Poloidal Array at one toroidal location in a passive stabilizer gap, about 4 cm beyond the major radius of the graphite tiles on the plasma facing side of the passive stabilizers. Each of the stainless steel coupons were partially coated with a 0.4 μm layer of graphite so as to provide measurements of both deposition and erosion. Deuterium implanted from the plasma in the carbon of the coupons was consistent with saturation by particles of a few hundred eV [10]. The change in carbon thickness was measured using a 1.5 MeV proton Rutherford back-scattering spectroscopy (RBS) before and after plasma exposure [10]. The results indicate net carbon erosion of all coupons. In the case of the poloidal coupon array, more carbon erosion occurred on the lower passive plate (0.17–0.25 μm) than on the upper passive plate (0.02–0.1 μm) coupons. In the case of the toroidal coupon array, on the outer vessel wall, the carbon erosion varied from ~ 0.06 to ~ 0.33 μm [10]. This toroidal asymmetry may be related in part to the shadowing and reflection effects of nearby hardware. Erosion of wall coupons was also observed on JET and attributed to effect of charge exchange neutrals [11]. Metal deposition (mainly Fe and Cu) was found on all coupons. In the case of the poloidal coupon array, more metal was found on the lower passive stabilizer coupons $(1.2–1.5 \times 10^{17}$ cm$^{-2})$ than on the upper $(\sim 0.5 \times 10^{17}$ cm$^{-2})$ [10]. This asymmetry may be attributable to the effect of the first CHI plasma experiments which were initiated across the lower divertor gap region; single null ohmic plasma discharges may have also contributed.

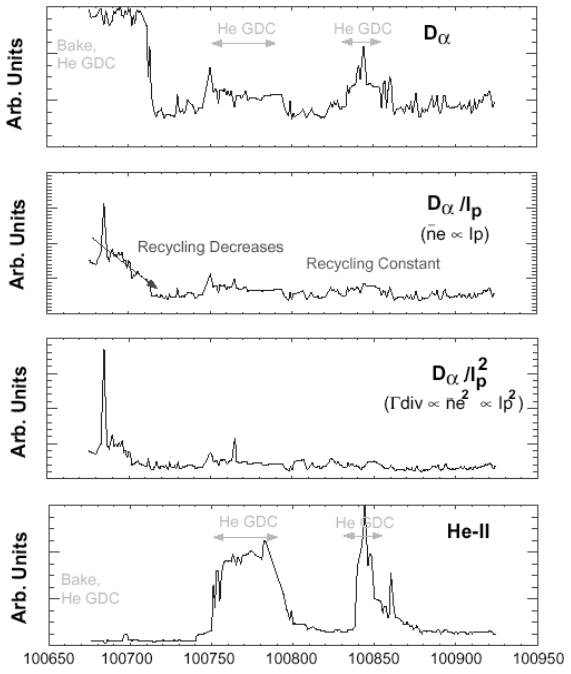

Fig. 4. Edge luminousity behavior of Da and He II for HeGDC sequences (refer to text).

2 MeV ^{4}He RBS and electron microscopy were used to measure metal deposition on four lower passive plate graphite tiles [10]. Fe and Cu were observed in rough areas (local depressions) on the plasma facing surfaces at $\sim 2 \times 10^{17}$ cm^{-2}, similar to the metal coverage on the lower passive stabilizer coupons.

Center column erosion was studied by implanting two center column tiles (one graphite and one CFC) with 300 keV Si to a depth of 0.34 μm. Ion beam analysis was performed before and after exposure to NSTX plasmas during the August 1999 experimental campaign. 2 MeV ^{4}He RBS measurements found the Si markers to be absent, thereby indicating net erosion exceeding >0.4 μm. In addition, metallic deposition of 0.13×10^{17} cm^{-2} was found on the graphite tile and 0.48×10^{17} cm^{-2} on the CFC tile which is about 10× less metal than deposited on the outer wall coupons and passive plate tiles [10]. This difference may be due to higher erosion rates on the center column than on outer coupons which were more distant from the plasma edge.

There was no macroscopic damage to the graphite tiles of the center column, inner and outer divertors, and the passive plates other than symmetric discoloration on plasma-facing, power-absorbing surfaces and a few arc

spots. In general, the visible changes to these plasma facing surfaces were toroidally symmetric but different for the lower and upper divertors. The lower outer divertor exhibited thermal deposition pattern extending from the divertor gap to its major radius center, however, the upper outer divertor tile surfaces exhibited a more centralized thermal deposition pattern. The upper divertor pattern may be indicative of normal double null ohmic plasma depositions, whereas the lower divertor pattern may be due to the sum effects of single null plasmas, double null plasmas, and CHI startup across the lower divertor gap region. The CHI ceramic insulators in the divertor gaps showed evidence of arcing and depositions which may be reduced in future experiments with the installation of boron nitride baffles [8].

In contrast to the graphite tile surface changes described above, the CFC tiles exhibited from about 2 to 8, horizontal damage tracks per tile. These tracks have the visual appearance of cracks but were actually shallow tracks about 0.1 cm wide by 0.01 cm deep and varying in length from about 0.5 to 3 cm. Some tracks are uniformly deep, others appear to be a series of pits. The axes of these tracks seem parallel to the carbon fibers embedded in the CFC material. Indeed the tiles were machined so that the CFC fibers were oriented parallel to the plasma facing side. However, due to the curvature of the tile surface, fiber ends appeared at the surface. These exposed ends of near surface fibers may have accelerated the erosion of fibers. In addition, microstresses in thin layers covering near-surface produced by machining may have caused some fibers to fracture under cyclic thermal stress. In the case of a typical track size of 0.5 cm long by 0.1 cm wide by 0.01 cm deep, a typical track volume of $\sim 5 \times 10^{-4}$ cm^3 would have released about 1 mg, or 5×10^{19} atoms of carbon into the plasma edge. This CFC behavior will be monitored during forthcoming NBI operations which will result in much higher power loading on these tiles.

5. Conclusions

NSTX progressed from First plasma to 1 MA discharges in a relatively short time using bakeout, D_2GDC, and HeGDC for wall conditioning. These results indicate that NSTX has a sound design. D_2GDC was found to be more effective at evolving water and hydrocarbons than HeGDC. HeGDC was found to be effective for removing remaining D_2. Inter-shot HeGDC allows fast recovery from an air vent, and CHI discharges. Inter-discharge HeGDC does not routinely improve performance; this may be due to the need for yet cleaner wall conditions. Net non-uniform carbon erosion and metal deposition (Cu and Fe) on passive stabilizer plate and midplane wall coupons. Heavier depositions were observed in the lower half of the vessel. This suggests CHI (initiated across the lower divertor gap) was the source for this asymmetry rather than GDC or plasma discharges. This effect may be reduced with the installation of additional graphite shielding.

Acknowledgements

This work is supported by US DoE Contracts DE-AC02-76CH03073, DE-AC05-00R22725, DE-FG02-99ER54524, DE-AC04-94AL85000, and DE-FG03-99ER54519.

References

[1] M. Bell et al., to appear in Proceedings of the European Physical Society Conference on Controlled Fusion and Plasma Physics, Budapest, Hungary, 12–16 June, 2000.
[2] Y-K.M. Peng, D. Strickler, Nucl. Fus. 26 (1986) 769.
[3] S.M. Kaye et al., Fus. Technol. 36 (1999) 16, and references therein.
[4] R. Maingi, Proceedings of the International Workshop on ST's, Abingdon, United Kingdom, 1996.
[5] R. Maingi, Proceedings of the International Workshop on ST's, St. Petersburg, Russia, 1997.
[6] H.W. Kugel et al., Proceedings of the 18th Symposium On Fusion Engineering, Albuquerque, NM, 25–29 October, 1999, IEEE, p. 296.
[7] J. Menard et al., to appear in Proceedings of 18th IAEA Fusion Energy Conference, Sorrento, Italy, 4–10 October, 2000.
[8] R. Raman et al., to appear in Proceedings of 18th IAEA Fusion Energy Conference, Sorrento, Italy, 4–10 October, 2000.
[9] D. Stutman et al., Bull. A. Phys. Soc. 44 (7) (1999) 187.
[10] W. Wampler et al., to be published.
[11] M. Mayer et al., J. Nucl. Mater 266–269 (1999) 604.